Results on the Spin-Dependent Scattering of Weakly Interacting Massive Particles on Nucleons from the Run 3 Data of the LUX Experiment

D. S. Akerib,[1,2,3] H. M. Araújo,[4] X. Bai,[5] A. J. Bailey,[4,*] J. Balajthy,[6] P. Beltrame,[7] E. P. Bernard,[8] A. Bernstein,[9] T. P. Biesiadzinski,[1,2,3] E. M. Boulton,[8] A. Bradley,[1] R. Bramante,[1,2,3] S. B. Cahn,[8] M. C. Carmona-Benitez,[10] C. Chan,[11] J. J. Chapman,[11] A. A. Chiller,[12] C. Chiller,[12] A. Currie,[4] J. E. Cutter,[13] T. J. R. Davison,[7] L. de Viveiros,[14] A. Dobi,[15] J. E. Y. Dobson,[16] E. Druszkiewicz,[17] B. N. Edwards,[8] C. H. Faham,[15] S. Fiorucci,[15] R. J. Gaitskell,[11] V. M. Gehman,[15] C. Ghag,[16] K. R. Gibson,[1] M. G. D. Gilchriese,[15] C. R. Hall,[6] M. Hanhardt,[5,18] S. J. Haselschwardt,[10] S. A. Hertel,[19,8,15] D. P. Hogan,[19] M. Horn,[19,8,15] D. Q. Huang,[11] C. M. Ignarra,[2,3] M. Ihm,[19,15] R. G. Jacobsen,[19,15] W. Ji,[1,2,3] K. Kazkaz,[9] D. Khaitan,[17] R. Knoche,[6] N. A. Larsen,[8] C. Lee,[1,2,3] B. G. Lenardo,[13,9] K. T. Lesko,[15] A. Lindote,[14] M. I. Lopes,[14] D. C. Malling,[11] A. Manalaysay,[13] R. L. Mannino,[20] M. F. Marzioni,[7] D. N. McKinsey,[19,8,15] D.-M. Mei,[12] J. Mock,[21] M. Moongweluwan,[17] J. A. Morad,[13] A. St. J. Murphy,[7] C. Nehrkorn,[10] H. N. Nelson,[10] F. Neves,[14] K. O'Sullivan,[15,19,8] K. C. Oliver-Mallory,[19,15] R. A. Ott,[13] K. J. Palladino,[22,2,3] M. Pangilinan,[11] E. K. Pease,[19,8,15] P. Phelps,[1] L. Reichhart,[16] C. Rhyne,[11] S. Shaw,[16] T. A. Shutt,[1,2,3] C. Silva,[14] V. N. Solovov,[14] P. Sorensen,[15] S. Stephenson,[13] T. J. Sumner,[4] M. Szydagis,[21] D. J. Taylor,[18] W. Taylor,[11] B. P. Tennyson,[8] P. A. Terman,[20] D. R. Tiedt,[5] W. H. To,[1,2,3] M. Tripathi,[13] L. Tvrznikova,[19,8,15] S. Uvarov,[13] J. R. Verbus,[11] R. C. Webb,[20] J. T. White,[20] T. J. Whitis,[1,2,3] M. S. Witherell,[10] F. L. H. Wolfs,[17] K. Yazdani,[4] S. K. Young,[21] and C. Zhang[12]

(LUX Collaboration)

[1]*Case Western Reserve University, Department of Physics, 10900 Euclid Ave, Cleveland, Ohio 44106, USA*
[2]*SLAC National Accelerator Laboratory, 2575 Sand Hill Road, Menlo Park, California 94205, USA*
[3]*Kavli Institute for Particle Astrophysics and Cosmology, Stanford University, 452 Lomita Mall, Stanford, California 94309, USA*
[4]*Imperial College London, High Energy Physics, Blackett Laboratory, London SW7 2BZ, United Kingdom*
[5]*South Dakota School of Mines and Technology, 501 East St Joseph St., Rapid City, South Dakota 57701, USA*
[6]*University of Maryland, Department of Physics, College Park, Maryland 20742, USA*
[7]*SUPA, School of Physics and Astronomy, University of Edinburgh, Edinburgh EH9 3FD, United Kingdom*
[8]*Yale University, Department of Physics, 217 Prospect St., New Haven, Connecticut 06511, USA*
[9]*Lawrence Livermore National Laboratory, 7000 East Ave., Livermore, California 94551, USA*
[10]*University of California Santa Barbara, Department of Physics, Santa Barbara, California 93106, USA*
[11]*Brown University, Department of Physics, 182 Hope St., Providence, Rhode Island 02912, USA*
[12]*University of South Dakota, Department of Physics, 414E Clark St., Vermillion, South Dakota 57069, USA*
[13]*University of California Davis, Department of Physics, One Shields Ave., Davis, California 95616, USA*
[14]*LIP-Coimbra, Department of Physics, University of Coimbra, Rua Larga, 3004-516 Coimbra, Portugal*
[15]*Lawrence Berkeley National Laboratory, 1 Cyclotron Rd., Berkeley, California 94720, USA*
[16]*Department of Physics and Astronomy, University College London, Gower Street, London WC1E 6BT, United Kingdom*
[17]*University of Rochester, Department of Physics and Astronomy, Rochester, New York 14627, USA*
[18]*South Dakota Science and Technology Authority, Sanford Underground Research Facility, Lead, South Dakota 57754, USA*
[19]*University of California Berkeley, Department of Physics, Berkeley, California 94720, USA*
[20]*Texas A&M University, Department of Physics, College Station, Texas 77843, USA*
[21]*University at Albany, State University of New York, Department of Physics, 1400 Washington Avenue, Albany, New York 12222, USA*
[22]*University of Wisconsin-Madison, Department of Physics, 1150 University Avenue, Madison, Wisconsin 53706, USA*

We present experimental constraints on the spin-dependent WIMP (weakly interacting massive particle)-nucleon elastic cross sections from LUX data acquired in 2013. LUX is a dual-phase xenon time projection chamber operating at the Sanford Underground Research Facility (Lead, South Dakota), which is designed to observe the recoil signature of galactic WIMPs scattering from xenon nuclei. A profile likelihood ratio analysis of 1.4×10^4 kg day of fiducial exposure allows 90% C.L. upper limits to be set on the WIMP-neutron (WIMP-proton) cross section of $\sigma_n = 9.4 \times 10^{-41}$ cm^2 ($\sigma_p = 2.9 \times 10^{-39}$ cm^2) at 33 GeV/c^2. The spin-dependent WIMP-neutron limit is the most sensitive constraint to date.

The weakly interacting massive particle (WIMP) is one of the leading candidates for explaining the observed abundance of dark matter in the Universe [1]. Astronomical evidence for the existence of dark matter ranges from galactic to cosmological scales [2–4]. However, its exact composition remains unknown. WIMPs arise in many extensions of the standard model of particle physics and are expected to have a small coupling to ordinary matter [5]. The Large Underground Xenon (LUX) experiment is designed to detect the low-energy scattering of galactic WIMPs with atomic nuclei.

LUX is a dual-phase xenon time projection chamber (TPC) with 250 kg active mass, currently operating at the Sanford Underground Research Facility (SURF) in Lead, South Dakota [6]. A WIMP interaction in the detector gives a low energy nuclear recoil ($\lesssim 100$ keV), producing prompt scintillation light ($S1$) and ionization electrons. An applied electric field (180 V/cm between the cathode and gate electrodes) drifts the electrons upwards into the gaseous phase of the detector, where they produce electroluminescence ($S2$). Photons are detected by two arrays of photomultiplier tubes (PMTs). The difference in arrival time between the $S1$ and $S2$ signals gives the depth of the interaction, and the (x, y) position is found from the localization of the $S2$ in the top PMT array. The ability to reconstruct positions of interactions in three dimensions allows fiducialization of the active volume, avoiding higher background regions near the detector walls and enabling rejection of multiple scatters. Electronic recoils (ER) are distinguished from nuclear recoil (NR) interactions by the ratio of the charge ($S2$) and scintillation ($S1$) signals.

LUX published world-leading limits on the spin-independent (SI) WIMP-nucleon scattering cross section from an exposure of 1.1×10^4 kg day in 2013 [7], for WIMP masses above 5.7 GeV. After collecting these data, a low energy NR calibration [8] was performed with a Deuterium-Deuterium (DD) neutron generator. This allows the charge and light response to be evaluated down to 1.1 keV, below the 3 keV recoil energy cutoff imposed in the original analysis. In addition, high statistics ER calibration data were acquired with a tritium source dissolved in the active liquid xenon [9], improving the characterization of the detector response to low energy ER interactions. A further 10 live days of WIMP search data were added taking the exposure up to 95 live days (1.4×10^4 kg day). Other improvements were made to the background model, vertex reconstruction, and event selection. These improvements motivated a reanalysis of the 2013 data, enhancing the sensitivity of the LUX experiment [10]. The SI result is compatible with the background-only hypothesis and sets a 90% confidence upper limit on the WIMP-nucleon cross section of 5.6×10^{-46} cm^2 at a WIMP mass of 33 GeV/c^2. Now we use the reanalyzed data to also set limits on the spin-dependent (SD) WIMP-proton and WIMP-neutron scattering cross sections.

The case for an axial-vector (spin-dependent) interaction is well motivated and occurs in various theories beyond the standard model of particle physics, including supersymmetry [11], universal extra dimensions [12], and little Higgs theories [13,14]. For the nonrelativistic velocities of galactic WIMPs, the scattering is mostly coherent across the whole nucleus. For isospin-conserving interactions, this leads to an enhancement of the scalar (spin-independent) interaction proportional to A^2. For the SD case, there is cancellation between the spins of nucleon pairs so the A^2 enhancement is not present. Therefore, nuclei with even numbers of protons and neutrons have almost zero nuclear spin, giving a negligible contribution to the SD interaction. However, models exist where the SI interaction is suppressed [15], making it essential to search for the SD interaction, and moreover, xenon is sensitive to this interaction because it contains isotopes with nonzero spin.

SI and SD are not the only possible interactions. In a general, nonrelativistic effective field theory treatment, there are several possible operators [16]. In particular, there are two ways in which WIMPs can couple to spin, with the projection of the spin either parallel or perpendicular to the momentum transfer. The standard SD response is a linear combination of these, only including operators which are nonvanishing at zero momentum transfer. Constraints on the complete set of operators will be presented in a future publication.

For direct detection experiments, the principal measured quantity is the standard WIMP-nucleus cross section σ_0. The WIMP-nucleus differential cross section for momentum transfer q for the SD interaction can be written in terms of σ_0 [17]:

$$\frac{d\sigma}{dq^2} = \frac{8G_F^2}{(2J+1)v^2} S_A(q) = \frac{\sigma_0}{4\mu_N^2 v^2} \frac{S_A(q)}{S_A(0)}, \qquad (1)$$

where G_F is the Fermi constant, μ_N is the WIMP-nucleus reduced mass, J is the total nucleus spin, v is the WIMP velocity relative to the target, and S_A is the spin structure function. S_A is analogous to the form factor in the SI case; it describes the spin distribution within the nucleus. All momentum dependence is contained in the $S_A(q)$ term. In order to compare direct detection experiments with different target nuclei, the WIMP-nucleon cross section is required. For $q = 0$, S_A reduces to:

$$S_A(0) = \frac{(2J+1)(J+1)}{4\pi J}|(a_0 + a_1')\langle S_p \rangle$$
$$+ (a_0 - a_1')\langle S_n \rangle|^2, \qquad (2)$$

where $\langle S_{p,n} \rangle$ are the proton or neutron spin expectation values averaged over the nucleus and $a_{0,1}$ are the isoscalar and isovector couplings. These are related to the WIMP couplings to protons and neutrons by $a_0 = a_p + a_n$ and $a_1 = a_p - a_n$. Then, $a_1' = a_1(1 + \delta a_1(0))$ includes the

effects of two-body currents in the δ term (most previous analyses have not included 2-body currents, which simplifies this equation), which represent couplings between a WIMP and two nucleons [18]. In this zero-momentum transfer limit, we can separate the two cases of "proton-only" ($a_0 = a_1 = 1$) or "neutron-only" ($a_0 = -a_1 = 1$) couplings and write:

$$\sigma_{p,n} = \frac{3\mu_{p,n}^2(2J+1)}{4\pi\mu_N^2}\frac{\sigma_0}{S_A(0)}. \qquad (3)$$

$S_A(q)$ can be obtained from detailed nuclear shell model calculations. The result depends on which nuclear states are included and the allowed configurations of nucleons within those states. There are also differences in the nuclear interactions accounted for. The calculation used here is from Klos et al. [17]. It includes the largest number of states and allowed configurations compared to previous theoretical treatments in the literature. The order of the experimentally measured nuclear energy levels in xenon is reproduced well. In addition, the Klos et al. result uses a chiral effective field theory treatment of the nuclear interactions including two-body currents. These structure functions are an update of those in Ref. [19]. Within the recoil energy range of interest, changes to the neutron-only structure function are small: at most 5% for ^{129}Xe and a maximum 20% increase for ^{131}Xe. For proton-only, the structure function is smaller than previously: as the recoil energy increases the difference in ^{129}Xe rises to 30% and in ^{131}Xe to 50%. We also compare to the structure function calculation of Ressell and Dean with the Bonn A nucleon-nucleon potential [20], which has been extensively used in previous SD results. This includes the same states as Ref. [17], but has more truncations in the allowed configurations of nucleons and only includes interactions with one nucleon.

There are two naturally occurring xenon isotopes with an odd number of neutrons, ^{129}Xe and ^{131}Xe (abundances 29.5% and 23.7%, respectively). Therefore, the "neutron-only" sensitivity is much higher than "proton-only", as the majority of the nuclear spin is carried by the unpaired neutron. When only WIMP interactions with one nucleon are considered, the choice of $a_{p,n}$ above corresponds to WIMPs either coupling to only protons or neutrons. However, once two-body currents are included, an interaction between a WIMP, a proton, and the unpaired neutron can occur even in the "proton-only" case. Therefore, this gives a significant enhancement to the structure function for "proton-only" coupling, while only slightly reducing the "neutron-only".

Single scatter events (one $S1$ followed by one $S2$) within the fiducial volume (radius < 20 cm, 38–205 μs drift time, or 48.6–8.5 cm above bottom PMT faces in z) are selected for the analysis. A total of 591 events are observed in the region of interest (cf. Fig. 2 in Ref. [10]) during an exposure

of 1.4×10^4 kg day. The background rate originating from NR events is negligible [10] but ER events produce a significant background. The ER backgrounds include external gamma rays from detector materials, ^{127}Xe x rays, and contaminants in the xenon (^{85}Kr, Rn) [21]. The tritium data set allows Monte Carlo simulations [22] to be tuned to ER calibration data, which is then used to generate PDFs (in $S1$ vs $S2$) for these ER backgrounds. Another important background comes from radon daughter decays on the PTFE walls of the TPC, with the tail of the distribution in reconstructed radius extending into the fiducial volume [23]. In these "wall events" some electrons are lost, resulting in a reduced $S2$ signal, so that many events lie below the signal band in $S2/S1$. Part of this background is ERs, which can mimic NRs due to their reduced $S2$ signal.
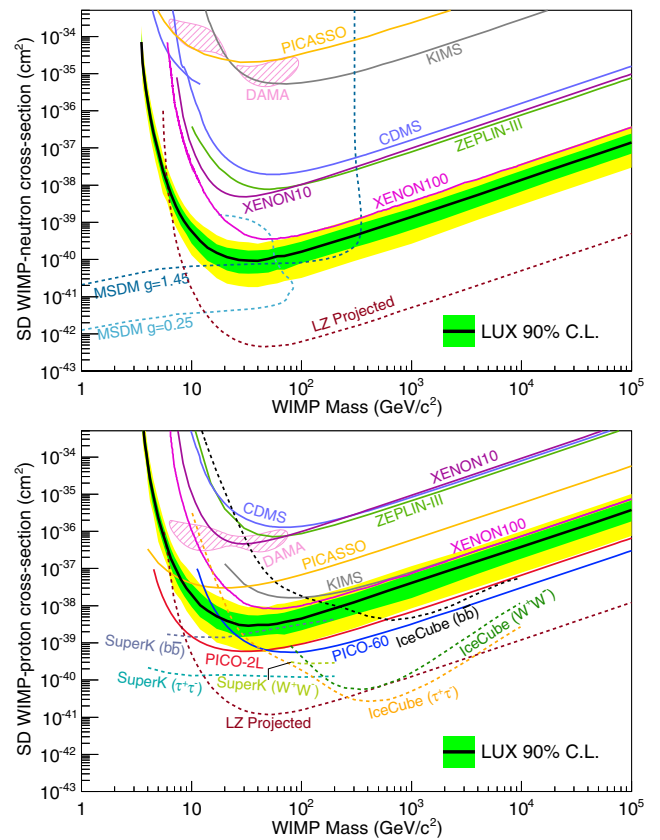

FIG. 1. LUX upper limits on the WIMP-neutron (top) and -proton (bottom) elastic SD cross sections at 90% C.L. The observed limit is shown in black with the $\pm 1\sigma$ ($\pm 2\sigma$) band from simulated background-only trials in green (yellow). Also shown are the 90% C.L. from: CDMS [29], KIMS [30,31], PICASSO [32], PICO-2L [26], PICO-60 [27], XENON10 [33], XENON100 [34], and ZEPLIN-III [35,36]. The DAMA allowed region at 3σ as interpreted in [28] without ion channeling is the shaded areas. Three indirect limits from IceCube [37] and SuperK [38] are shown. Collider limits from CMS monojet searches are included, assuming the MSDM model with two coupling scenarios [39]. The projected sensitivity for the LZ experiment is shown for an exposure of 5.6×10^5 kg day [40].

There are also NR wall events from the alpha decay of ^{210}Po, which produces a recoiling daughter ^{206}Pb nucleus. The PDF model for the wall events is generated from sidebands in the data.

For SD scattering the signal spectrum (per unit cross section) is suppressed relative to the SI case. The shape of the recoil spectrum produced by a SD neutron-only interaction is very similar to that from a SI one. The SD proton interaction produces a somewhat harder recoil spectrum at all WIMP masses, with the effect growing for heavier WIMPs; at 20 TeV, the SD proton-only has 28% of recoils between 25 and 50 keV, compared to 20% for SI. The signal PDF for a given WIMP mass is evaluated by fitting the yield of single scatters from the DD-neutron calibration in $S2$ and $S1$ [8]. Systematic uncertainties from the DD neutron calibration are included in this fit. Contributions from the different isotopes are accounted for by adding their differential event rates. Confidence intervals are set with a profile likelihood ratio (PLR) in four variables: $S1$, $S2$, radius, and height. All of these variables

are useful for discriminating signal from background. Further detail on the analysis can be found in Refs. [10,24], including the application of a power constraint at the median sensitivity so as not to benefit from background fluctuations. The observed events are consistent with the expectation from background only.

The upper limits on the SD WIMP-nucleon cross sections from the PLR analysis are shown in Fig. 1. The minimum excluded cross section at 90% C.L. for WIMP-neutron (WIMP-proton) elastic scattering is $\sigma_n = 9.4 \times 10^{-41}$ cm^2 ($\sigma_p = 2.9 \times 10^{-39}$ cm^2), for a WIMP mass of 33 GeV/c^2. For the neutron-only coupling the excluded cross section is lower than from previous direct searches. The proton-only limit is less constraining by a factor of ∼30. Using alternative structure functions from Ref. [20], the neutron-only upper limit is improved by a factor ∼0.5 and the proton-only degraded by ∼2.5. The results presented here improve on the limits set in Ref. [25] owing mostly to the lower energy threshold and the better background rejection afforded by the PLR-based statistical
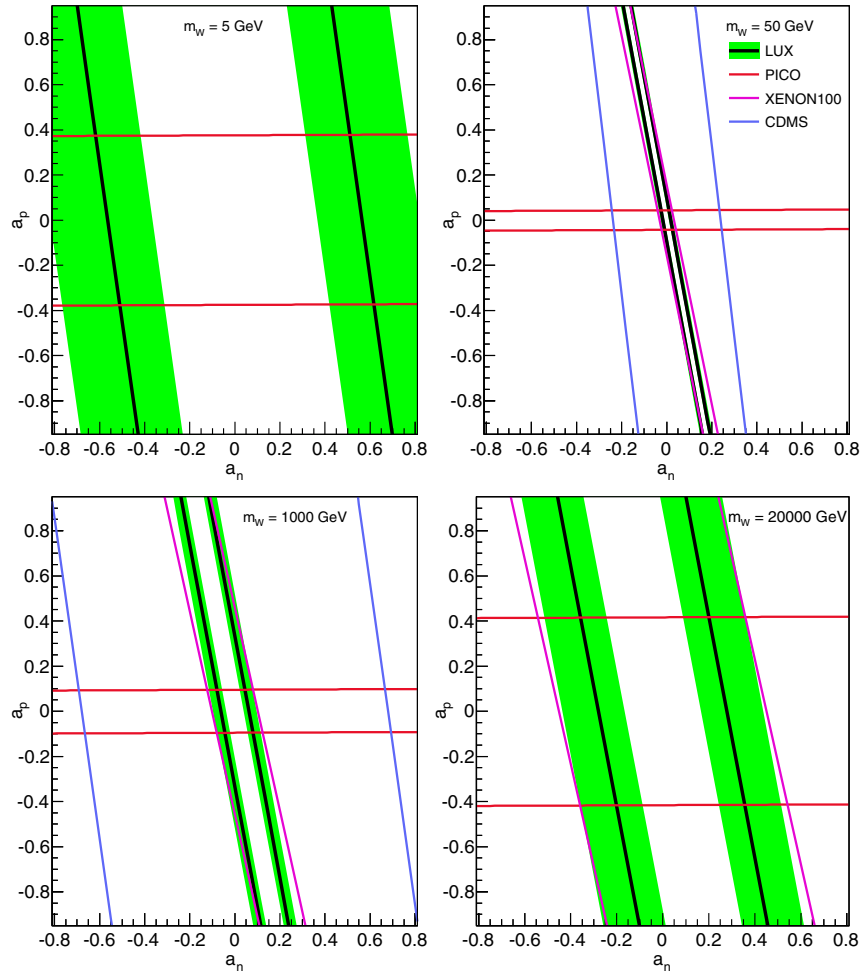

FIG. 2.   Constraints on the effective WIMP couplings to protons and neutrons, a_p and a_n, at 90% C.L. for various WIMP masses (5, 50, 1000, 20000 GeV). Also shown are CDMS [44], PICO-2L (for 5 GeV) [26], PICO-60 (for other masses) [27], and XENON100 [34], where the constraints have been inferred from the limits on $\sigma_{p,n}$ using the method in Ref. [43].

analysis. PICO [26,27] is more sensitive to proton-only coupling, due to the unpaired proton of the fluorine nuclei in the C_3F_8 target. However, the inclusion of two-body currents in the xenon structure functions yields significant proton-only sensitivity and the proton-only limit from this result is competitive. The DAMA allowed region [28] is excluded even in the proton-only case by this result.

Collider searches for dark matter particles can be interpreted in the same parameter space as direct searches for particular conditions [39]. In Fig. 1, we include limits from CMS monojet searches [41], assuming the minimal simplified dark matter (MSDM) model for the particular case where the couplings of the mediator to the quarks and the dark matter particle are equal ($g = g_q = g_{DM}$). The cross section is dependent on these couplings, so we compare to the smallest and largest values used in Ref. [39]. For low WIMP masses, the collider limits are stronger for both couplings, but these searches are not sensitive to heavier WIMPs. It is important to note this interpretation of collider searches is model dependent. Therefore, dark matter signals would ideally be observed in collider, indirect, and direct searches in order to fully investigate the interactions of WIMPs.

With limits set on $\sigma_{p,n}$ the allowed region in $a_p - a_n$ space can be found following the procedure detailed in [42]:

$$\sum_A \left(\frac{a_p}{\sqrt{\sigma_p^A}} \pm \frac{a_n}{\sqrt{\sigma_n^A}} \right)^2 > \frac{\pi}{24 G_F^2 \mu_p^2}, \qquad (4)$$

where $\sigma_{p,n}^A$ are the limits on the proton or neutron-only cross sections, for the isotope with mass number A. The excluded region is shown in Fig. 2. Typically, only the most sensitive channel of the two cross sections is shown. In this case, the limits in the $a_p - a_n$ plane can be found following the method detailed in Ref. [43], which is a good approximation if $a_p \gg a_n$ or vice versa.

This result improves the constraint on a_n over previous experiments. The lines are parts of elongated ellipses and the orientation depends on the sensitivity to both a_p and a_n. The angle of the ellipse for LUX and XENON100 is not the same due to differences in the spin structure functions used and the energy scale in the analysis (which affects the signal spectrum). XENON100 also had slightly different abundances of ^{129}Xe and ^{131}Xe, due to the addition of isotopically modified xenon. This plot also emphasizes the complementarity between the different detector materials.

In conclusion, we have set the most stringent limits on the SD WIMP-neutron cross section for all WIMP masses down to 3.5 GeV/c^2 from the 2013 LUX data, and the proton-only limit is also competitive. We also improve the constraints on the possible values of the couplings a_p and a_n, complementary to experiments that are more sensitive to the proton than the neutron coupling. The sensitivity to both proton and neutron-only coupling will be improved greatly with future large-scale experiments with xenon targets such as LZ [40].

[*]Corresponding author.
a.bailey12@imperial.ac.uk.

[1] J. L. Feng, Annu. Rev. Astron. Astrophys. **48**, 495 (2010).
[2] J. I. Read, J. Phys. G **41**, 063101 (2014).
[3] D. Harvey, R. Massey, T. Kitching, A. Taylor, and E. Tittley, Science **347**, 1462 (2015).
[4] Planck Collaboration, arXiv:1502.01589.
[5] A. K. Drukier, K. Freese, and D. N. Spergel, Phys. Rev. D **33**, 3495 (1986).
[6] D. S. Akerib *et al.*, Nucl. Instrum. Methods Phys. Res., Sect. A **704**, 111 (2013).

[7] D. S. Akerib *et al.*, Phys. Rev. Lett. **112**, 091303 (2014).

[8] D. S. Akerib *et al.* (to be published).

[9] D. S. Akerib *et al.*, arXiv:1512.03133.

[10] D. S. Akerib *et al.*, preceding Letter, Phys. Rev. Lett. **116**, 161301 (2016).

[11] G. Jungman, M. Kamionkowski, and K. Griest, Phys. Rep. **267**, 195 (1996).

[12] D. Hooper and S. Profumo, Phys. Rep. **453**, 29 (2007).

[13] A. Birkedal-Hansen and J. G. Wacker, Phys. Rev. D **69**, 065022 (2004).

[14] J. Hubisz and P. Meade, Phys. Rev. D **71**, 035016 (2005).

[15] V. A. Bednyakov, H. V. Klapdor-Kleingrothaus, and S. G. Kovalenko, Phys. Rev. D **50**, 7128 (1994).

[16] A. L. Fitzpatrick, W. Haxton, E. Katz, N. Lubbers, and Y. Xu, J. Cosmol. Astropart. Phys. 02 (2013) 004.

[17] P. Klos, J. Menéndez, D. Gazit, and A. Schwenk, Phys. Rev. D **88**, 083516 (2013).

[18] E. Epelbaum, H.-W. Hammer, and U.-G. Meißner, Rev. Mod. Phys. **81**, 1773 (2009).

[19] J. Menéndez, D. Gazit, and A. Schwenk, Phys. Rev. D **86**, 103511 (2012).

[20] M. T. Ressell and D. J. Dean, Phys. Rev. C **56**, 535 (1997).

[21] D. S. Akerib *et al.*, Astropart. Phys. **62**, 33 (2015).

[22] D. S. Akerib *et al.*, Nucl. Instrum. Methods Phys. Res., Sect. A **675**, 63 (2012).

[23] C. Lee, Ph.D. thesis, Case Western Reserve University, 2015.

[24] D. S. Akerib *et al.* (to be published).

[25] C. Savage, A. Scaffidi, M. White, and A. G. Williams, Phys. Rev. D **92**, 103519 (2015).

[26] C. Amole *et al.*, Phys. Rev. D **93**, 061101 (2016).

[27] C. Amole *et al.*, Phys. Rev. D **93**, 052014 (2016).

[28] C. Savage, G. Gelmini, P. Gondolo, and K. Freese, J. Cosmol. Astropart. Phys. 04 (2009) 010.

[29] Z. Ahmed *et al.*, Phys. Rev. Lett. **106**, 131302 (2011).

[30] H. Lee *et al.*, Phys. Rev. Lett. **99**, 091301 (2007).

[31] S. C. Kim *et al.*, Phys. Rev. Lett. **108**, 181301 (2012).

[32] S. Archambault *et al.*, Phys. Lett. B **711**, 153 (2012).

[33] J. Angle *et al.*, Phys. Rev. Lett. **101**, 091301 (2008).

[34] E. Aprile *et al.*, Phys. Rev. Lett. **111**, 021301 (2013).

[35] D. Y. Akimov *et al.*, Phys. Lett. B **709**, 14 (2012).

[36] V. Lebedenko *et al.*, Phys. Rev. Lett. **103**, 151302 (2009).

[37] M. Aartsen *et al.*, arXiv:1601.00653.

[38] K. Choi *et al.*, Phys. Rev. Lett. **114**, 141301 (2015).

[39] S. A. Malik *et al.*, Phys. Dark Univ. **9–10**, 51 (2015).

[40] LZ Collaboration, arXiv:1509.02910.

[41] CMS Collaboration, Eur. Phys. J. C **75**, 235 (2015).

[42] D. Tovey, R. Gaitskell, and P. Gondolo, Phys. Lett. B **488**, 17 (2000).

[43] F. Giuliani and T. A. Girard, Phys. Rev. D **71**, 123503 (2005).

[44] Z. Ahmed *et al.*, Phys. Rev. Lett. **102**, 011301 (2009).